Supplementary Information

Effective electronic tuning of Pt single atoms via heterogeneous atomic coordination of (Co,Ni)$(OH)_2$ for efficient hydrogen evolution

An Pei,[a, 1] Ruikuan Xie,[c, 1] Yun Zhang,[a, 1] Yingliang Feng,[a, 1] Weizhen Wang,[d] Sifan Zhang,[a] Zinan Huang,[e] Lihua Zhu,[a, b, *] Guoliang Chai,[c, g, *] Zhiqing Yang,[d, *] Qingsheng Gao,[e] Hengqiang Ye,[d] Congxiao Shang,[b] Bing Hui Chen,[f] Zhengxiao Guo[b, *]

[a] Jiangxi Provincial Key Laboratory of Functional Molecular Materials Chemistry, College of Chemistry and Chemical Engineering, Faculty of Materials Metallurgy and Chemistry, Jiangxi University of Science and Technology, Ganzhou 341000, Jiang Xi, China

[b] HKU-CAS Joint Laboratory on New Materials and Department of Chemistry, The University of Hong Kong, Hong Kong SAR, China

[c] State Key Laboratory of Structural Chemistry, Fujian Institute of Research on the Structure of Matter, Chinese Academy of Sciences (CAS), Fuzhou, 350002 Fujian, China.

[d] Ji Hua Laboratory, Foshan 528200, China

[e] College of Chemistry and Materials Science, and Guangdong Provincial Key Laboratory of Functional Supramolecular Coordination Materials and Applications, Jinan University, Guangzhou 510632, China

[f] College of Chemistry and Chemical Engineering, Xiamen University, Xiamen 361005, China

[g] Fujian Science & Technology Innovation Laboratory for Optoelectronic Information of China Fuzhou, Fujian 350108, P. R. China

Hongqi Road No. 86, Zhanggong District, Ganzhou 341000, Jiang Xi, China

Corresponding Authors

zhulihua@jxust.edu.cn (Lihua Zhu); g.chai@fjirsm.ac.cn (Guoliang Chai); yangzhq@jihualab.ac.cn (Zhiqing Yang); zxguo@hku.hk (Zhengxiao Guo).

[1] These authors contributed equally to this work.

Experimental methods

Materials preparation

The (Co,Ni)$(OH)_2$/C catalyst was prepared via a precipitation method. Firstly, a calculated amount of $NiCl_2 \cdot 6H_2O$ and $CoCl_2 \cdot 6H_2O$ precursors was mixed into 16.5 mL of deionized water (N_2-saturated) and stirred for 0.5 h at room temperature. Then, 2.5 mL ethanol was added to form a uniform coordination compound. The solution was kept N_2-saturated by continuing bubbled N_2. After 10 min, Carbon (0.3 g) was added to the mixture. The as-prepared N_2-saturated NaOH (99.9%) solution was injected into the mixed solution quickly to deposit (Co,Ni)$(OH)_2$ on carbon. After sealed and vigorous stirring for 10 h, the (Co,Ni)$(OH)_2$/C catalyst was obtained by filtration and washed with the deionized water several times. The $Co(OH)_2$/C and $Ni(OH)_2$/C catalyst were synthesized with the same method by change the precursors of $NiCl_2 \cdot 6H_2O$ and $CoCl_2 \cdot 6H_2O$.

The series of the Pt/(Co,Ni)$(OH)_2$/C catalysts were synthesized via an electrodeposition strategy by controlling the deposition time. The electrodeposition experiments were conducted with the standard three-electrode system using CHI 760e Instrument. Carbon paper (1×1 cm^2) covered (Co,Ni)$(OH)_2$/C (3 mg, ethanol: water = 9:1, ultrasound for 30 min) dropped with 40 μL 0.25 wt% Nafion solution were used as the working electrode, and 1 $mmol \cdot L^{-1}$ H_2PtCl_6 solution as the electrolyte for the Pt deposition. The saturated calomel electrode (SCE) with a salt bridge was used as the reference electrode, a graphite rod was applied as the counter electrode. After carbon paper covered (Co,Ni)$(OH)_2$/C was dried naturally, it was immersed in 1 $mmol \cdot L^{-1}$ H_2PtCl_6 solution, and the constant potentials of the electrodeposition process were -0.8 V (vs. SCE) for 10, 20, and 30 s, respectively. The carbon paper electrodeposited with Pt was washed with ultrapure water several times. After drying at room temperature, it was employed for the electrochemical measurements directly. The $Pt_1/Co(OH)_2$/C, $Pt_1/Ni(OH)_2$/C, and Pt_1/C were prepared by controlling the same electrodeposition time of 20 s but change the covered substrate.

Characterizations

Inductively coupled plasma optical emission spectrometry (ICP-OES) was performed on an Agilent

730 to accurately measure the practical content of the metals (*e.g.,* Pt, Co, Ni) in the samples. Aberration-corrected high-resolution transmission electron microscopy (Titan G2 60-300) was applied to reveal the morphology and nanostructure of different catalysts at 300 kV acceleration voltage. The Titan G2 60-300 was also applied to acquire the images of AC-STEM-EDS chemical elemental mapping of C, O, Ni, Co, and Pt with an acceleration voltage of 300 kV. The phase composition and structure of the catalysts were acquired through XRD measurements (Rigaku Ultima IV X-ray diffractometer) with Cu K_α as an X-ray source (λ=0.15406 nm). The surface element's valence state of the catalysts was analyzed via X-ray photoelectron spectroscopy spectrum on a PHI Quantum 200 to obtain the metal composition and atomic valence states of the surface. In the measurements, Al K_α (hv =1486.6 eV) was adopted as the target source to correct the binding energy of the catalysts, with the binding energy of C 1s as the internal standard.

Operando Raman spectra

The *Operando* Raman measurements were carried out employing a Horiba HR-800 Raman microspectrometer. The 1 × 1 cm^2 carbon paper-covered catalysts were adopted as the working electrode, a Hg/HgO was employed as reference electrodes and the counter electrodes were a graphite rod. A two-compartment electrochemical cell equipped with a proton exchange membrane (Nafion 117, Sigma-Aldrich) was used in a 1.0 M KOH solution. Combing with a CHI 650 electrochemical workstation, *Operando* Raman spectra at OCP and different applied potential (vs. Hg/HgO) for $Pt_1/(Co,Ni)(OH)_2/C$ and Pt_1/C were recorded with a typical electrochemical Raman spectroscopy setup in 1.0 M KOH.

Electrochemical measurements

All electrochemical measurements were carried out by electrochemical workstation CHI 760E using a three-electrode system with a carbon rod as the counter electrode, a saturated calomel electrode as a reference electrode and it was calibrated with another standard saturated calomel electrode (SCE) at open-circuit voltage before the electrochemical measurements. For the evaluation of double-layer capacitance (C_{dl}) towards different materials, the cyclic voltammetry (CV) was estimated at the potential range of 0.2 to 0.4 V (vs. RHE) at different scan rates from 20 to 100 $mV \cdot s^{-1}$. Besides, linear sweep voltammetry (LSV) curves were recorded with the potential from -0.6 to 0 V (vs. RHE) by a sweep rate of 5 $mV \cdot s^{-1}$. After the open-circuit voltage was determined, electrochemical impedance spectroscopy (EIS) was performed with a potential amplitude from low frequency (0.01 Hz) to high frequency (100 K Hz) to obtain the Nyquist plots. Moreover, two typical methods were both carried out to appraise the stability of the catalysts. One

was the continuous cyclic voltammetry, which was performed for 20000 cycles (sweep rate of 50 $mV \cdot s^{-1}$, 200 $mV \cdot s^{-1}$) from 0 V to -0.6 V (vs. RHE) and the other method was the chronoamperometry at 100 $mA \cdot cm^{-2}$ for 24 h.

Computational method

All the density functional theory (DFT) calculations were performed via the Vienna *Ab initio* Simulation Package (VASP),[1-3,] and the projector-augmented plane wave (PAW) pseudopotentials were used for the elements involved.[4] The generalized gradient approximation (GGA) of Perdew, Burke, and Ernzerhof (PBE) was used to treat the exchange-correlation of electrons.[5] The models of $(Co,Ni)(OH)_2$, $(Co,Ni)(OH)_2$ adsorbed with Pt single atom ($Pt_1/(Co,Ni)(OH)_2$) and Pt(111) slabs calculated in this study are shown in Fig.S17-19. The models for $Pt_1/Co(OH)_2$ and $Pt_1/Ni(OH)_2$ are the same as the $Pt_1/(Co,Ni)(OH)_2$ except for the elements in the hydroxides. The (001) facet is selected for all hydroxides in this study since they are layered structures along the (001) direction. A vacuum region larger than 15 Å was added along the direction normal to the slab plane to avoid the interaction between periodic supercells. The electron wave function was expanded in plane waves and a cutoff energy of 500 eV was selected. The Monkhorst-Pack meshes of ($3 \times 3 \times 1$) were adopted for the Brillouin zone (BZ) of the slabs.[6] The convergence in the energy and force were set to 10^{-4} eV and 0.01 eV/Å, respectively.

In this study, the hydrogen binding energy in Fig. 3i was calculated as:

$$\Delta E_H = E(*H) - E(H^+ + e^-) - E(*) \quad (1)$$

where E(*H), $E(H^+ + e^-)$ and E(*) were the total energy directly obtained by DFT calculations. $E(H^+ + e^-) = 1/2E(H_2)$ at 0 V vs. reversible hydrogen electrode (RHE) according to the computational hydrogen electrode (CHE) model which was proposed by Nørskov *et al*.[7,8]

The free energies of $H_2O(l)$ and $H_2(g)$ were used as references for the calculation of the free energies of reaction intermediates. The adsorption energy for the reaction intermediate is calculated as follows:[9]

$$\Delta G = \Delta E_{Total} + \Delta E_{ZEP} - T\Delta S + \Delta G_s \quad (2)$$

where ΔE_{Total} is the calculated adsorption total energy by DFT, ΔE_{ZPE} is zero-point energy, ΔS is entropy, and ΔG_s is solvation energy.[10-13]

Calculation of the surface density of single atoms and TOF of the catalysts

We calculated the surface density of single atoms (0.58 Pt atoms nm^{-2}) based on Pt loading measured by ICP-OES and the specific surface area of the catalyst. This method of estimating the density of single atoms has also been adopted by some recent publications.[14,15] The calculation process is given as follows:

Step 1. Calculation of the amount of Pt material on the electrode surface = (3 *10^{-3}g*1.41wt%)/(195.05 g/mol) = 1.8057*10^{-7} mol

(3 *10^{-3}g = sample weight, Pt loading =1.41wt%, molar mass of Pt = 195.05 g/mol)

Step 2. Calculation of the specific surface area of Pt_1 (electrochemical active area) in Pt_1/(Co,Ni)$(OH)_2$/C = (178.9-89.8)/0.04 = 2227.5 cm^2 = 2.2275*10^{17} nm^2,

(178.9 mF cm^{-2} and 89.8 mF $cm^{-2}$are the C_{dL} of Pt_1/(Co,Ni)$(OH)_2$/C and (Co,Ni)$(OH)_2$/C, respectively; the difference of [C_{dL}_Pt_1/(Co,Ni)$(OH)_2$/C - C_{dL}_(Co,Ni)$(OH)_2$/C] represents the contribution of Pt_1 to ECSA, the Cs of carbon-based materials = 0.04 mF cm^{-2})

Step 3. Calculation of the surface (area) density of the single atoms = 1.8057*10^{-7} mol* 6.02×10^{23}/(2.2275*10^{17} nm^2) = 0.58 Pt atoms nm^{-2}=5.8*10^{13} Pt atoms cm^{-2}

(1.8057*10^{-7} mol refers to the amount of Pt material on the electrode surface, 6.02×10^{23} was Avogadro constant (the number of Pt atoms in 1 mol Pt), 2.2275*10^{17} nm^2 represents the specific surface area of Pt_1)

The calculation method of turnover frequency (TOF, s^{-1}) of single-atom catalysts for the HER:

The turnover frequency (TOF, s^{-1}) of the catalysts for the HER, defined as the hydrogen evolution reaction (HER) rate per active site and per time, was derived from the following equation (1).[16-18]

$$TOF\ (s^{-1}) = \left\{ \frac{number\ of\ total\ hydrogen\ /\ cm^2\ of\ geometric\ area}{number\ of\ total\ active\ actives\ of\ /\ cm^2\ geometric\ area} \right\} \square\ \square \qquad (1)$$

Here, the current density (j) was derived from the current generated during the HER. The total number of hydrogens turn overs were calculated from the current density according to the following equation (2), and the TOF (s^{-1}) was obtained by equation (3).

$$\text{No. } H_2 = \left(\frac{|j|\ mA}{cm^2}\right)\left(\frac{1\ C\ cm^{-1}}{1000\ mA}\right)\left(\frac{1\ mol\ e^-}{96485.3\ C}\right)\left(\frac{1\ mol\ H_2}{2\ mol\ e^-}\right)\left(\frac{6.022\ \times 10^{23}\ H_2\ molecules}{1\ mol\ H_2}\right)$$

$$= |j| \times 3.12068 \times 10^{15} \frac{(H_2/s)}{cm^2} \text{ per } \frac{mA}{cm^2} \quad (2)$$

$$TOF\ (s^{-1}) = (|j| \times 3.12068 \times 10^{15} \frac{(H_2/s)}{cm^2} \text{ per } \frac{mA}{cm^2}) / N_{active} \quad (3)$$

For the single-atom catalyst model, the total number of Pt single-atoms on the electrode surface was obtained by the estimated ICP-OES analysis. Pt single atoms worked as an HER active site in DFT calculation. Thus, the total number of active actives geometric area (cm^{-2}) (N_{active}) was derived from the following equation (4).

$$N_{active} = 1/2 \times \left\{NA \times \frac{(m \times S \times wt\%)}{M}\right\} \quad (4)$$

Here, the *NA* was Avogadro constant (the number of Pt atoms in 1 mol Pt, 6.022×10^{23}), m is the loading of the catalyst on the electrode ($3*10^{-3}$ g cm^{-2} in our case), S is the geometric surface area of the working electrode (1 cm^2 in this work), The *wt*% of Pt was estimated by ICP-OES analysis, M is the molar mass of Pt = 195.05 g/mol

Table S1 Metal contents and atomic ratios in different catalysts measured by ICP-OES.

Entry	Catalyst	Metal loading (wt%)			Atomic ratios
		Pt/%	Co/%	Ni/%	
1	Pt/(Co,Ni)$(OH)_2$/C-10 s	0.81	6.28	6.03	1.9:49.9:48.1
2	Pt_1/(Co,Ni)$(OH)_2$/C-20 s	1.41	6.26	6.00	3.4:49.2:47.4
3	Pt/(Co,Ni)$(OH)_2$/C-30 s	3.67	6.25	6.02	8.3:46.6:45.1
4	Pt_1/Co$(OH)_2$/C	1.63	12.32	-	3.8:96.2
5	Pt_1/Ni$(OH)_2$/C	1.57	-	12.35	3.7:96.3
6	Pt_1/C	1.85	-	-	-

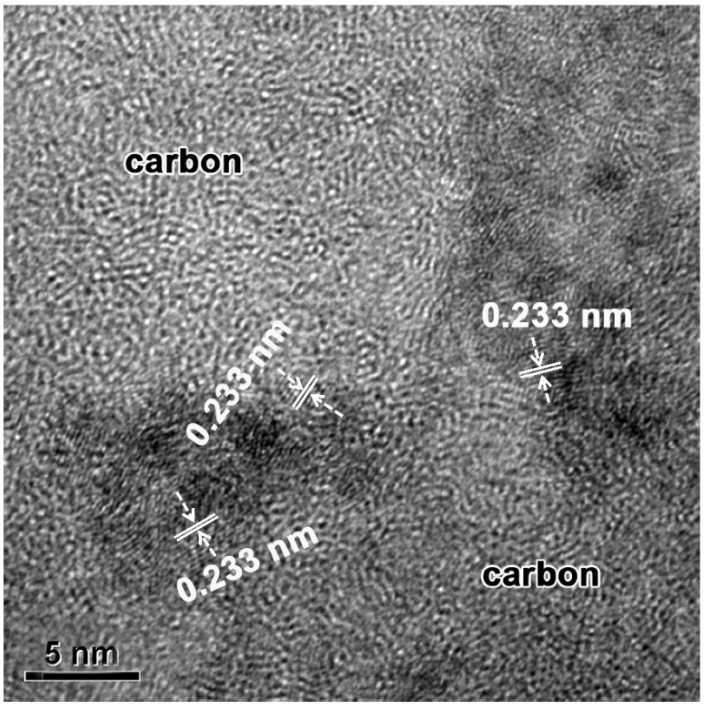

Fig. S1 The spacing of 0.233 nm matches well with the spacing between neighboring (101) planes for (Co,Ni)$(OH)_2$.

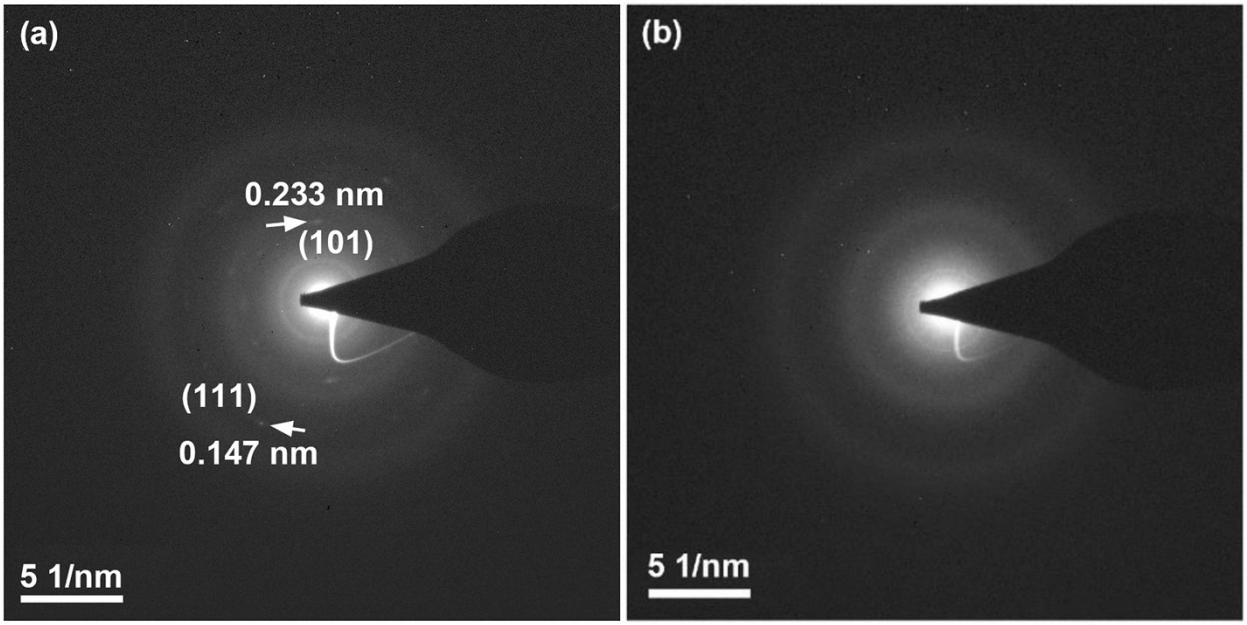

Fig. S2 (a) SAED patterns showing diffraction spots from (101) and (111) lattice planes of hydroxide. (b) SAED patterns for amorphous carbon support.

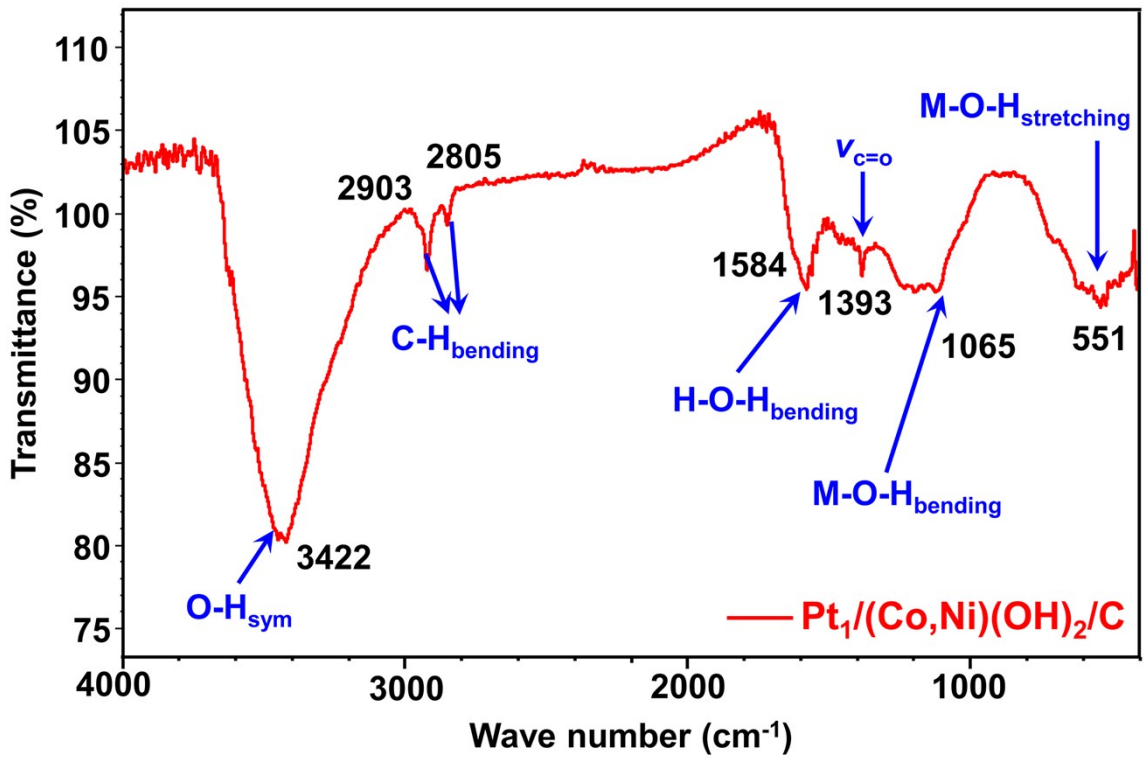

Fig. S3 FT-IR spectrum of $Pt_1/(Co,Ni)(OH)_2/C$ sample. To further confirm the presence of the hydroxide phase of $Pt_1/(Co,Ni)(OH)_2/C$ sample, the FT-IR analysis was conducted. According to the FT-IR results and the references, the infrared spectra were accurately attributed and the existence of hydroxides was confirmed. (*Int. J. Hydrogen Energy*, 2021, 46, 22789-22798. *Nanoscale*, 2019, 11, 12655-12671. *Electrochim. Acta* 2021, 368, 137633. *Chem. Eng. J.* 2020, 390, 124525.)

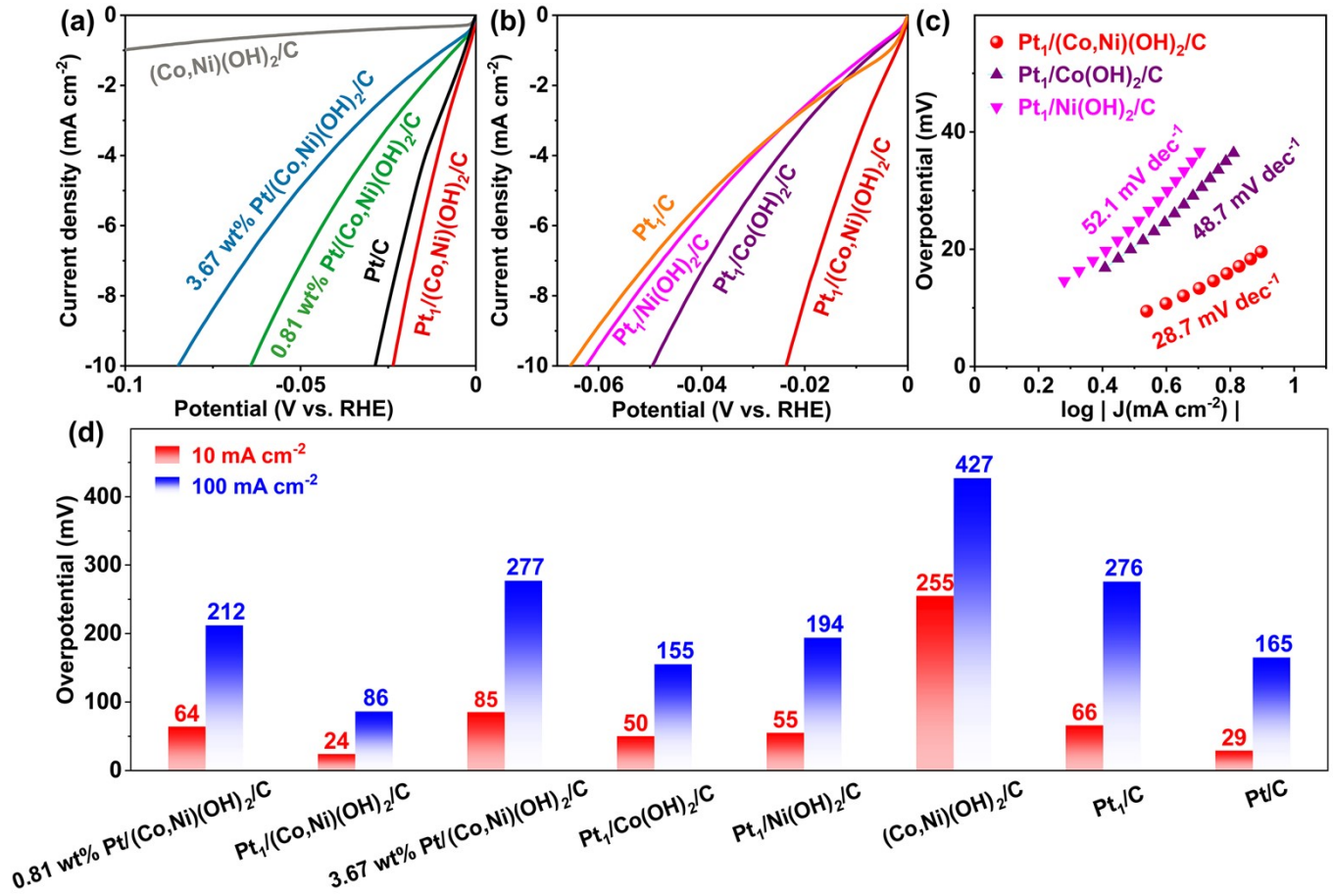

Fig. S4 The HER polarization curves: (a) 0.81 wt% Pt/(Co,Ni)(OH)$_2$/C, Pt$_1$/(Co,Ni)(OH)$_2$/C, 3.67 wt% Pt/(Co,Ni)(OH)$_2$/C, (Co,Ni)(OH)$_2$/C, and commercial 20 wt% Pt/C; (b) Pt$_1$/(Co,Ni)(OH)$_2$/C, Pt$_1$/Co(OH)$_2$/C, Pt$_1$/Ni(OH)$_2$/C, Pt$_1$/C in 1.0 M KOH solution at a current density of 10 mA cm^{-2}, the scan rate of 5 mV s^{-1}; (c) Tafel plots of Pt$_1$/(Co,Ni)(OH)$_2$/C, Pt$_1$/Co(OH)$_2$/C, Pt$_1$/Ni(OH)$_2$/C; (d) Comparison of the overpotentials of the as-prepared catalysts and commercial 20 wt% Pt/C at 10 and 100 mA·cm^{-2}, respectively.

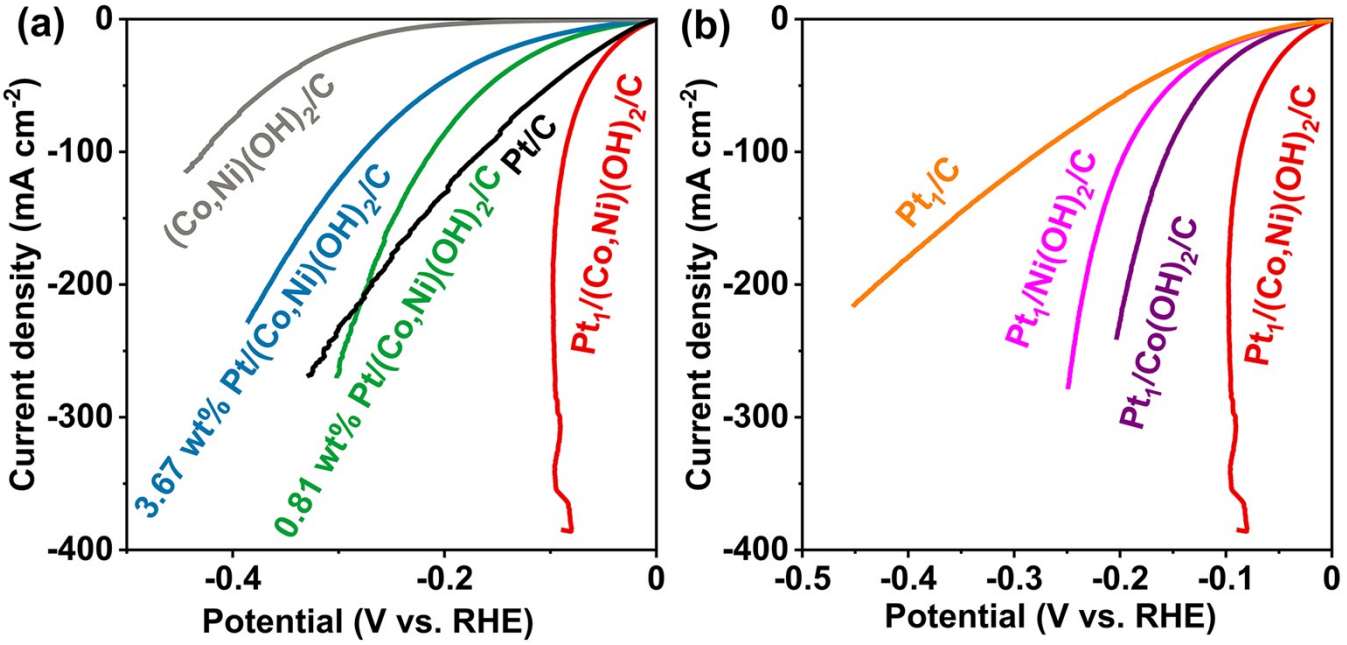

Fig. S5 HER polarization curves at a high current density range to 400 mA cm^{-2}: (a) as-synthesised Pt/$(Co,Ni)(OH)_2$/C catalysts with different Pt loading, $(Co,Ni)(OH)_2$/C, and commercial 20 wt% Pt/C; and (b) as-prepared Pt_1 catalysts of different types of support.

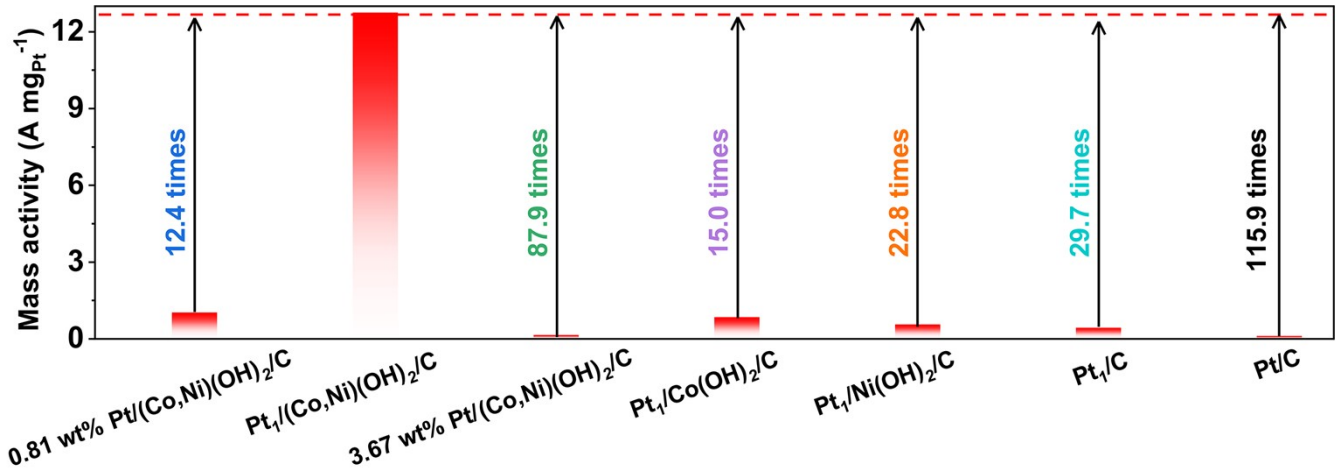

Fig. S6 The HER mass activity (normalized by the loading of Pt) towards the as-obtained catalysts and commercial 20 wt% Pt/C at polarization potential of -0.09 V.

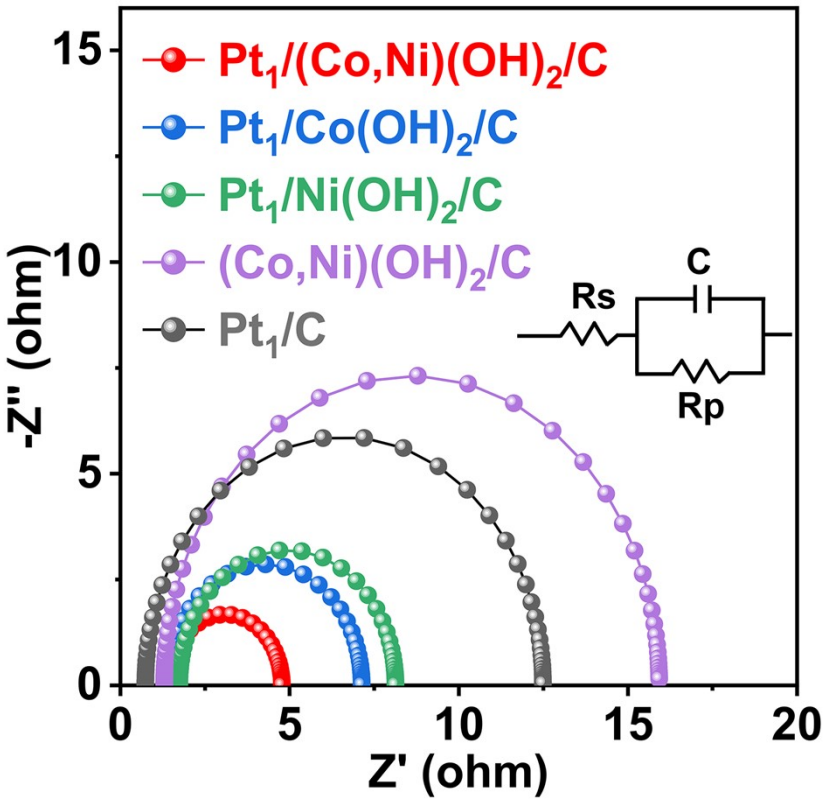

Fig. S7 Nyquist plots of as-obtained Pt Single atom catalysts and $(Co,Ni)(OH)_2/C$ substrate in 1.0 M KOH solution.

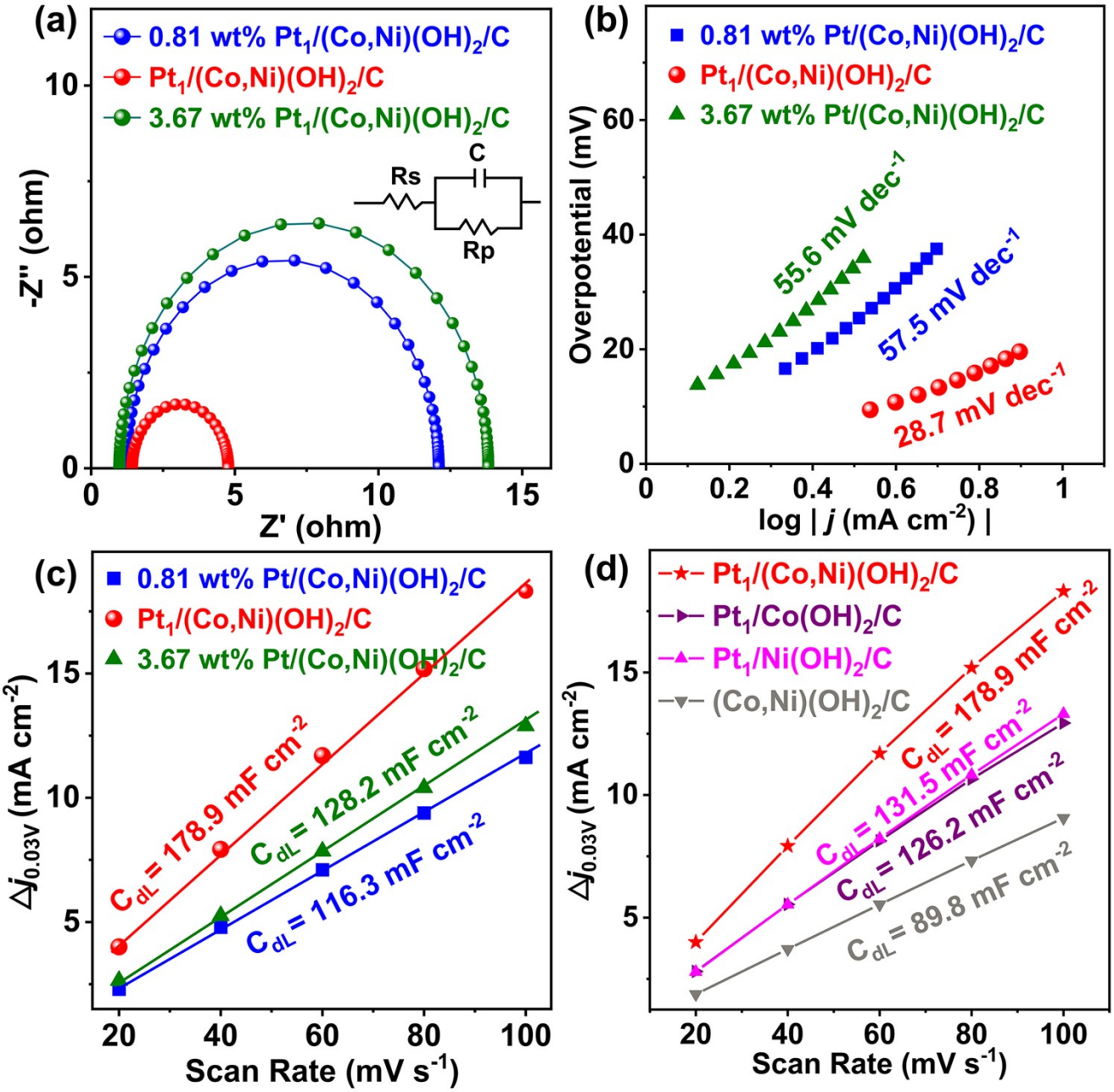

Fig. S8 (a) Nyquist plots; (b) Tafel plots; Linear fitting of the capacitive current versus the CV scanning rate: (c) 0.81 wt% Pt/(Co,Ni)$(OH)_2$/C, Pt_1/(Co,Ni)$(OH)_2$/C, and 3.67 wt% Pt/(Co,Ni)$(OH)_2$/C, and (d) Pt_1/(Co,Ni)$(OH)_2$/C, Pt_1/Co$(OH)_2$/C, Pt_1/Ni$(OH)_2$/C, and (Co,Ni)$(OH)_2$/C.

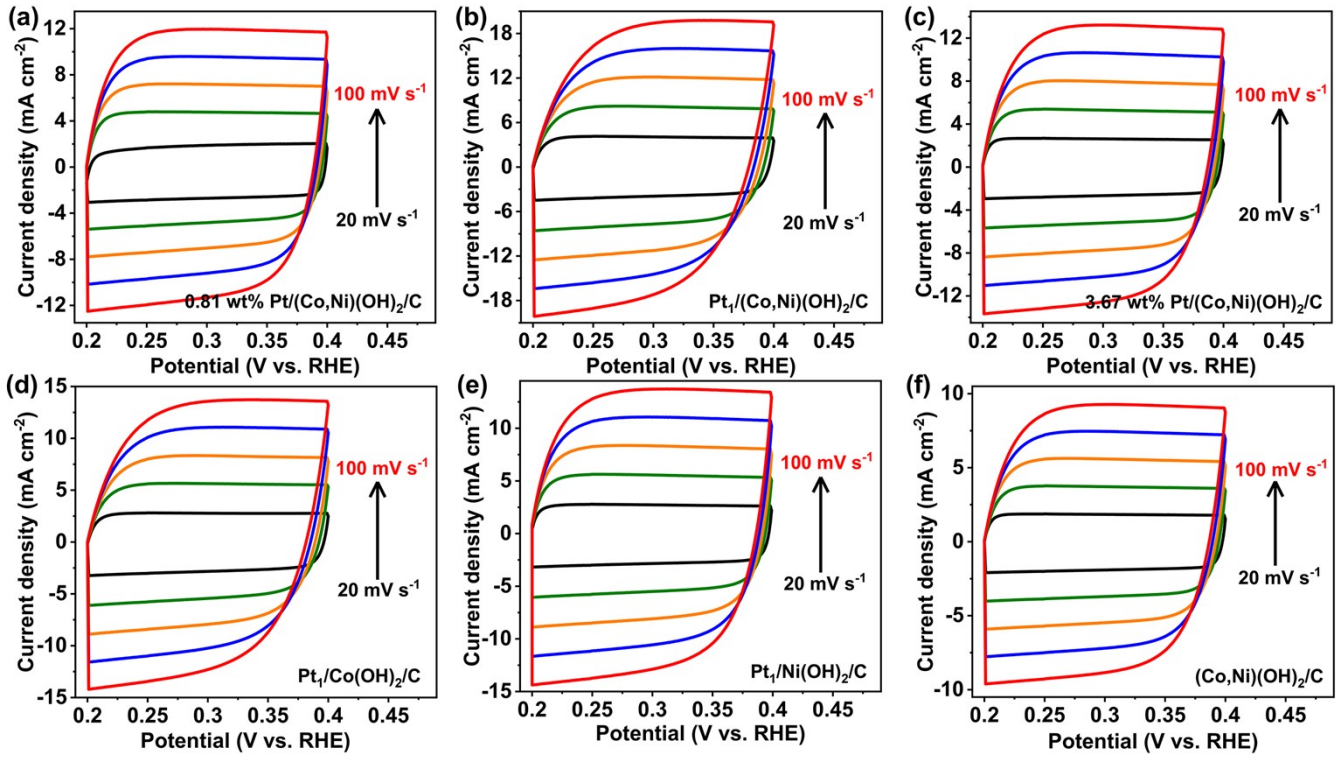

Fig. S9 CV curves of (a) 0.81 wt% Pt/(Co,Ni)$(OH)_2$/C, (b) Pt_1/(Co,Ni)$(OH)_2$/C, (c) 3.67 wt% Pt/(Co,Ni)$(OH)_2$/C, (d) Pt_1/Co$(OH)_2$/C, (e) Pt_1/Ni$(OH)_2$/C, and (f) (Co,Ni)$(OH)_2$/C in the region of 0.2 to 0.4 V (the Non-Faraday interval) with scanning rates from 20 to 100 mV·s^{-1}, used to calculate the ESCA.

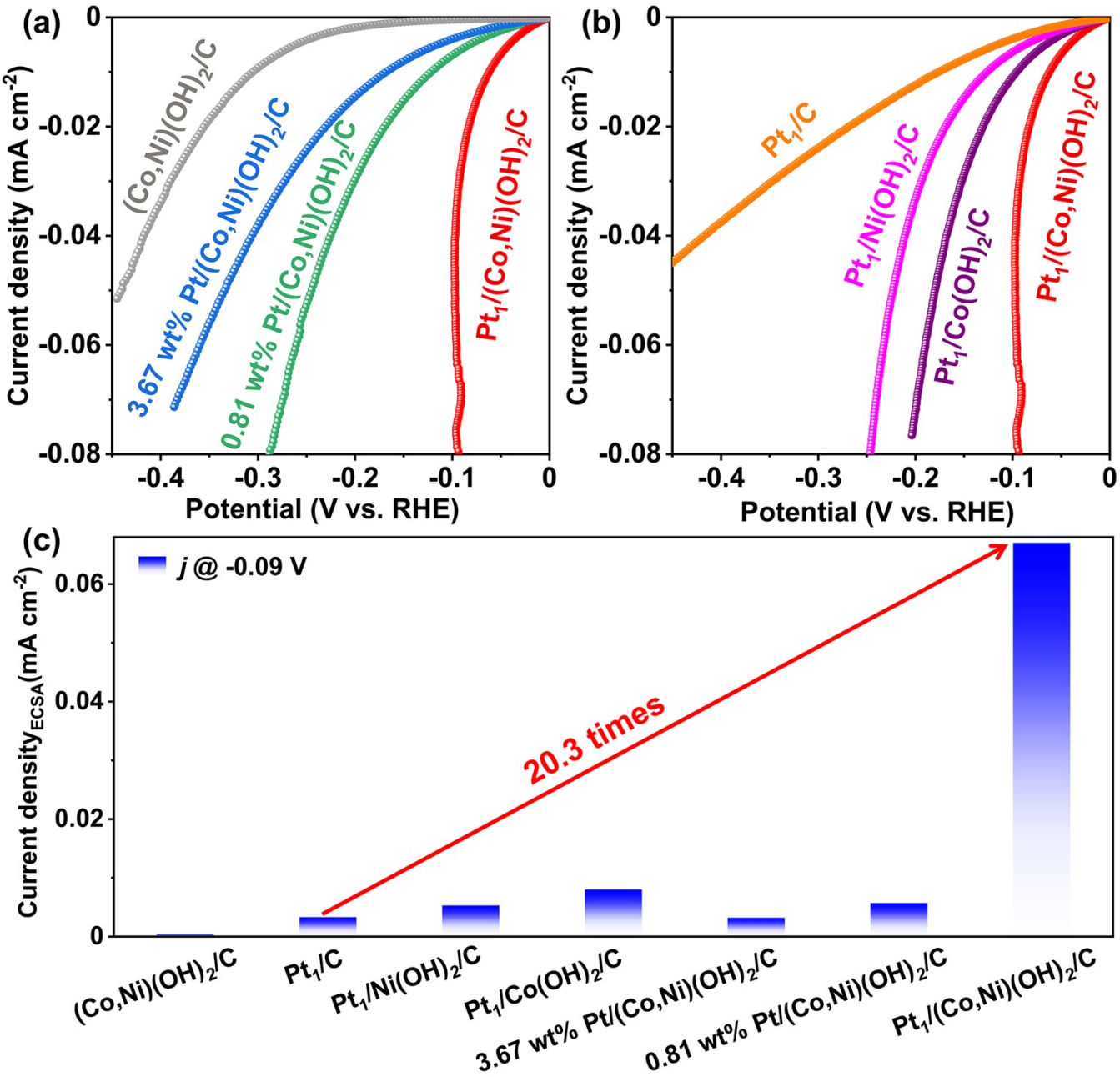

Fig. S10 The ECSA normalization for all the as-prepared catalysts.

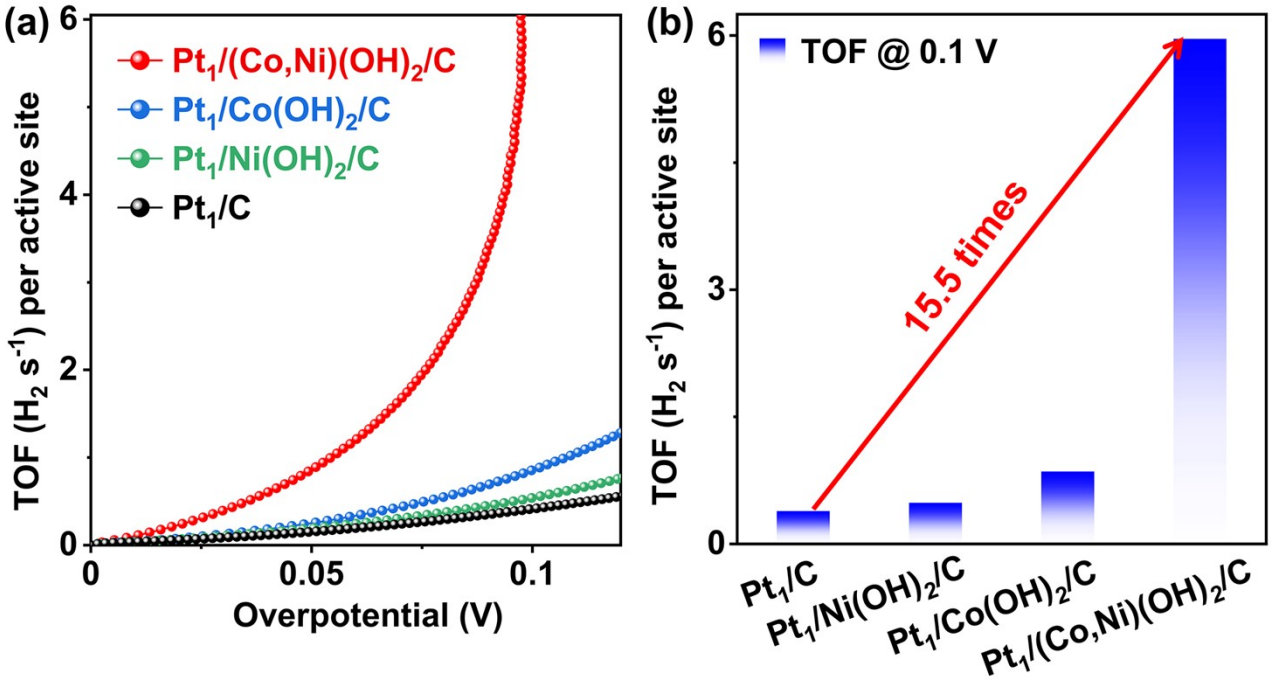

Fig. S11 (a) TOFs of the $Pt_1/(Co,Ni)(OH)_2/C$, $Pt_1/Co(OH)_2/C$, $Pt_1/Ni(OH)_2/C$, and Pt_1/C samples at an overpotential of 0 to 0.15 V. (b) Comparison of TOFs at an overpotential of 0.1 V.

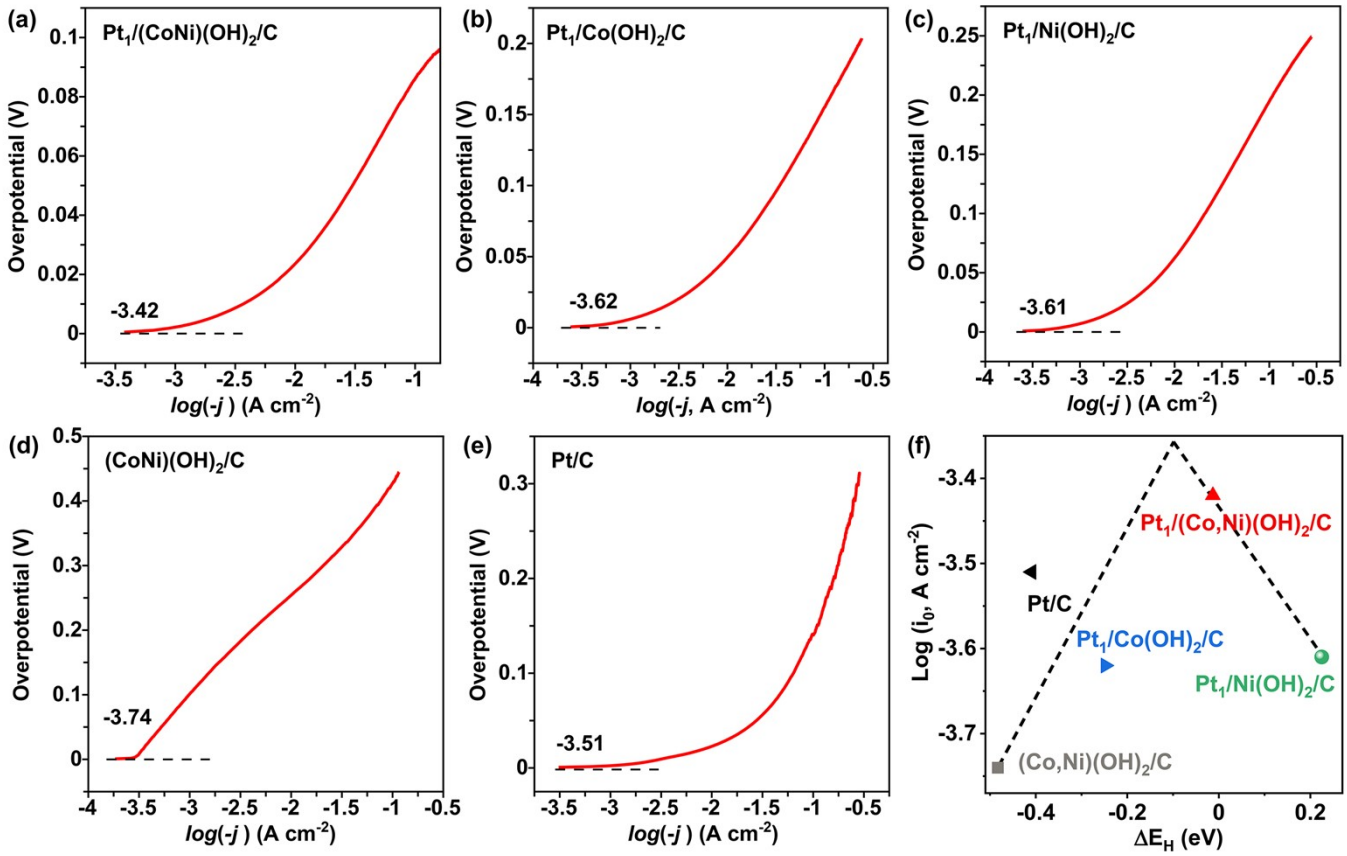

Fig. S12 (a-e) The Tafel plots of the samples. (f) Volcano plot of hydrogen adsorption free energy (ΔGH*) of different metal catalysts in HER.

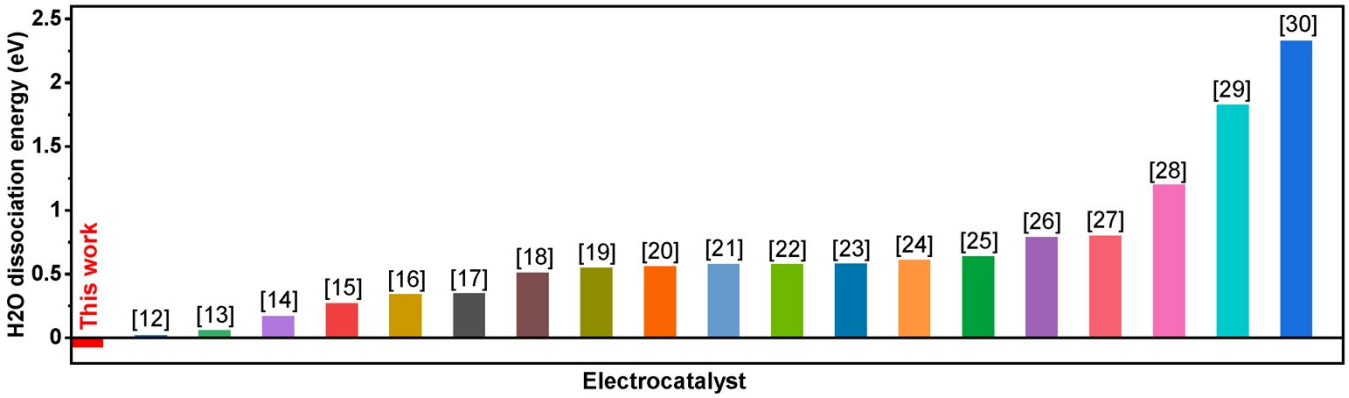

Fig. S13 Comparison of water dissociation energy of different reported catalysts including the $Co(OH)_2$ (0.02 eV)[19], Pt_1-C_2 (0.06 eV)[20], Ru-doped $SrTiO_3$ (0.17)[21], Co_3S_4 PNS_{vac} (0.27 eV)[22], O,Cu-CoPO nanowire (0.34 eV)[23], RhO_2 (0.35 eV)[24], α-MoC_{1-x} (0.51 eV)[25], Ru-N_4 (0.550 eV)[26], Mo exposed NiMoP (0.56 eV)[27], pyridinic-N-MoP (0.58 eV)[28], NiO/Pt (0.58 eV)[29], Cr-Co_4N (0.582 eV)[30], Mn-hcp Ni (0.61 eV)[31], MoS_2/LDH (0.64 eV)[32], 1T-MoS_2/SWNT (0.79 eV)[33], $CoNiS_2$ (0.80 eV)[34], GN_2@RuMo (1.2 eV)[35], MoS_2/$Ni(OH)_2$ (1.83 eV) [36], and Ni_3N (2.33 eV)[37].

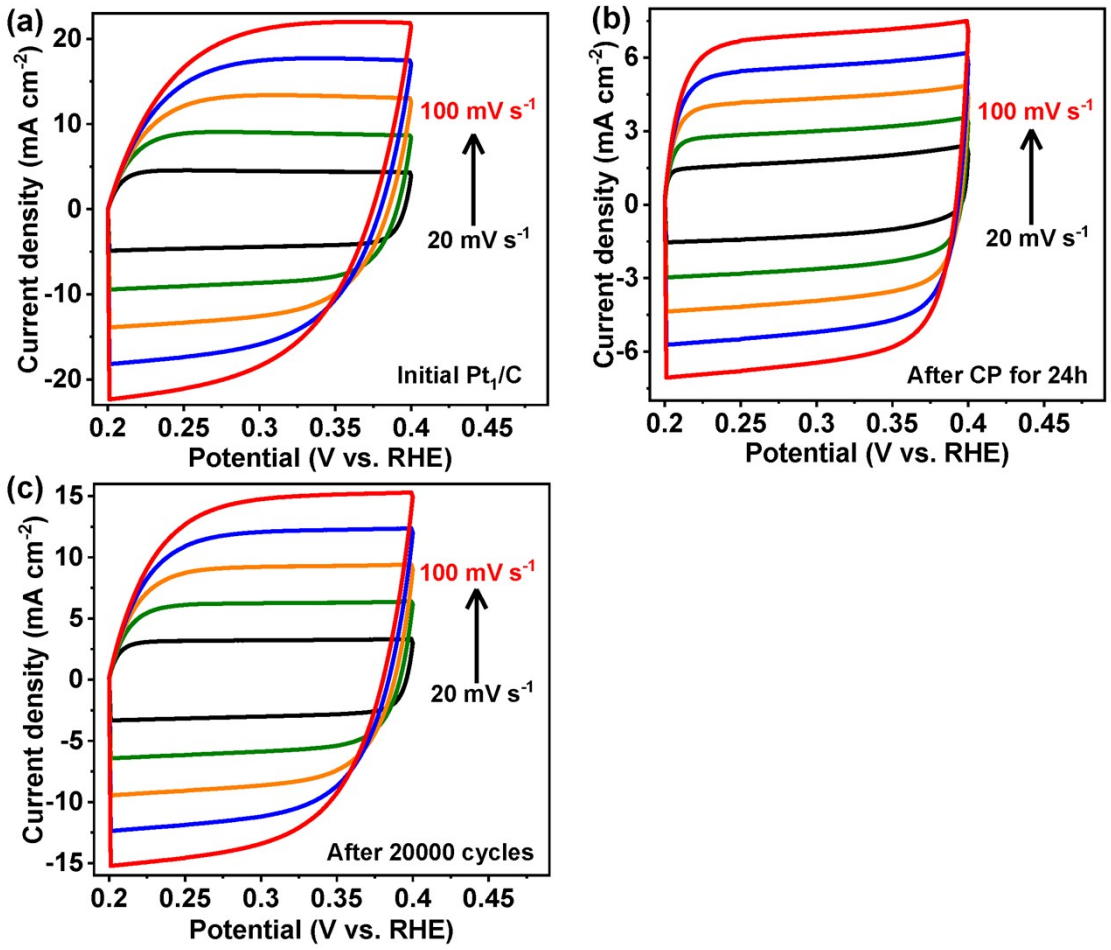

Fig. S14 CV curves in the region of 0.2 to 0.4 V with scan rates from 20 to 100 mV s^{-1} of (a) the initial Pt_1/C, (b) Pt_1/C after CP for 24 h, and (c) Pt_1/C after 20000 cycles HER measurements.

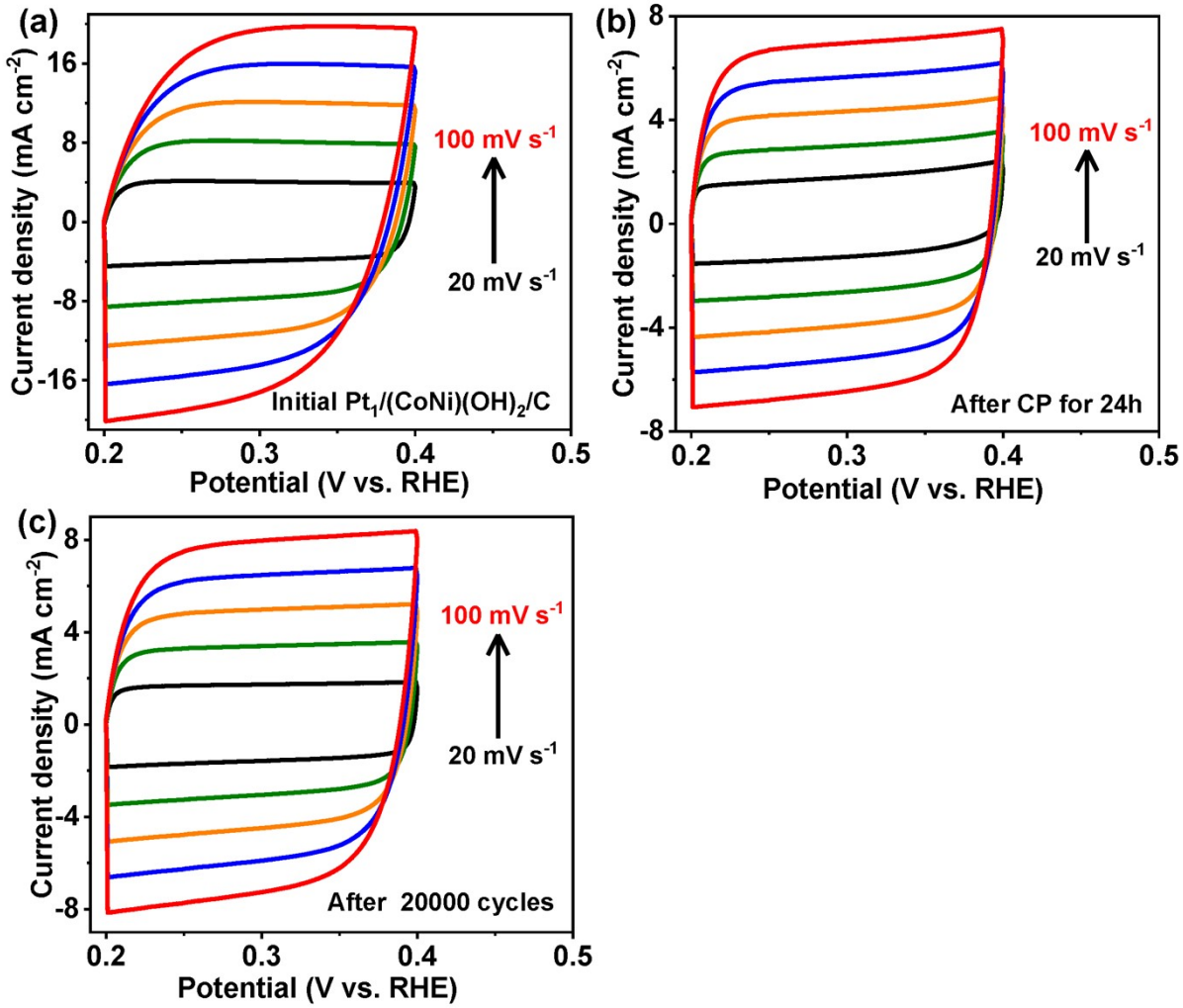

Fig. S15 CV curves in the region of 0.2 to 0.4 V with scan rates from 20 to 100 mV s^{-1} of (a) the initial $Pt_1/(Co,Ni)(OH)_2/C$, (b) $Pt_1/(Co,Ni)(OH)_2/C$ after CP for 24 h, (c) $Pt_1/(Co,Ni)(OH)_2/C$ after 20000 cycles HER measurements.

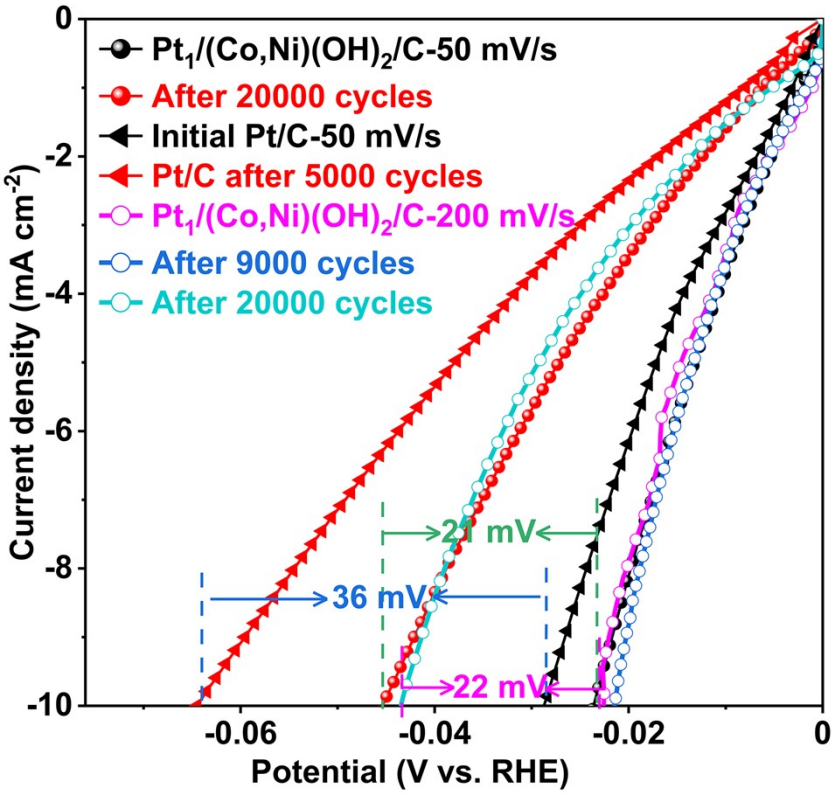

Fig. S16 Comparison of the effect of scanning rate at 50 and 200 mV s^{-1} towards the HER performance of $Pt_1/(Co,Ni)(OH)_2/C$ for 20000 cycles; and Pt/C at 50 mV s^{-1} for 5000 cycles.

Table S2 Comparison of the HER activities between $Pt_1/(Co,Ni)(OH)_2/C$ and other reported Pt single atomic electrocatalysts.

Electrocatalysts	Electrolyte	Pt_{SA} loading (wt%)	η_{10} (mV)	Tafel slope (mV dec^{-1})	References
$Pt_1/(Co,Ni)(OH)_2/C$	1.0 M KOH	1.41	24	28.7	This work
$Pt\text{-}_{SAs}/MoSe_2$	1.0 M KOH	4.70	29	34	*Nat. Commun.* **2021**, 12, 3021
$Pt\text{-}_{SAs}/MoS_2$	1.0 M KOH	5.10	65	50	
$Pt_{SA}\text{-}Mn_3O_4$	1.0 M KOH	2.00	24	54	*Energy Environ. Sci.* **2022**, doi.org/ 10.1039/D2EE02151J
$Pt_{SA}\text{-}Co(OH)_2$@Ag NWs	1.0 M KOH	2.8	29	35	*Energy Environ. Sci.* **2020**, 13, 3082-3092
$Pt_1/N\text{-}C$	1.0 M KOH	2.50	46	36.8	*Nat. Commun.* **2020**, 11, 1029
Pt_1@Fe-N-C	1.0 M KOH	2.10	108	-	*Adv. Energy Mater.* **2018**, 8, 1701345
Pt_{SA}-NiO/Ni	1.0 M KOH	1.14	26	27	*Nat. Commun.* **2021**, 12, 3783
$Pt_{SA}/S\text{-}C$	0.5 M H_2SO_4	5.00	53	46.9	*Nat. Commun.* **2019**, 10, 4977
$Pt_{SA}\text{-}Co(OH)_2$	1.0 M KOH	2.80	29	35.7	*Energy Environ. Sci.* **2020**, 13, 3082-3092
$Pt\text{-}_{SA}/TiO_2$	1.0 M KOH	1.10	-	410	*Chem. Eng. J.* **2022**, 427, 131309
$Mo_2TiC_2T_x\text{-}Pt_{SA}$	0.5 M H_2SO_4	1.20	30	30	*Nat. Catal.* **2018**, 1, 985

Table S3 Comparison of the HER activities between $Pt_1/(Co,Ni)(OH)_2/C$ and other reported advanced electrocatalysts.

Electrocatalysts	Electrolyte	η_{10} (mV)	η_{50} (mV)	Tafel slope (mV dec^{-1})	References
$Pt_1/(Co,Ni)(OH)_2/C$	1.0 M KOH	24	65	28.7	This work
Pt/MgO	1.0 M KOH	39	-	39	*Nat. Commun.* **2022**, 13, 2024
Pt/np-$Co_{0.85}Se$	1.0 M KOH	58	-	39	*Nat. Commun.* **2019**, 10, 1743.
IrCo@N-C	1.0 M KOH	45	-	80	*Adv. Mater.* **2018**, 30, 1705324
Pt/TiB_xO_y	1.0 M KOH	~200	-	135	*ACS Catal.* **2022**, 12, 5970-5978
RuCo@N-C	1.0 M KOH	28	-	31	*Nat. Commun.* **2017**, 8, 14969
Sr_2RuO_4	1.0 M KOH	61	-	51	*Nat. Commun.* **2019**, 10, 149
er-WS_2-Pt	1.0 M KOH	~48	-	65	*Adv. Mater.* **2018**, 30, 1704779
Ru@CN-0.16	1.0 M KOH	284	-	27.8	*Energy Environ. Sci.* **2018**, 11, 800
Pt@PCM	1.0 M KOH	139	-	73.6	*Sci. Adv.* **2018**, 4, eaao6657
Pt-SL/TiO_2	1.0 M KOH	210	-	79	*Small* **2021**, 17, 2100732
Pt-NiFe-LDH-0.5-12	1.0 M KOH	-	86	46	*Nano Energy* **2020**, 72, 104669
Ru/$Ni(OH)_2$/NF	1.0 M KOH	25	-	45	*J. Mater. Chem. A* **2019**,7, 11062-11068
Pt/NiRu-OH	1.0 M KOH	38	-	39	*Appl. Catal. B-Environ.* **2020**, 269, 118824
Pt-CoS_2/CC	1.0 M KOH	24	-	82	*Adv. Energy Mater.* **2018**, 8, 1800935
NiFe-LDH-Pt-ht/CC	1.0 M KOH	101	205	127	*Nano Energy* **2017**, 39, 30-43
NiFeIr-LDH	1.0 M KOH	34	-	32	*Chem. Commun.* **2018**, 54, 6400-6403
NiFeRu-LDH	1.0 M KOH	29	-	31	*Adv. Mater.* **2018**, 30, 1706279
RuP_2@NPC	1.0 M KOH	52	-	69	*Angew. Chem. Int. Ed.* **2017**, 56, 11559-11564
Pt/$Co(OH)_2$	1.0 M KOH	32	-	70	*ACS Catal.* **2017**, 7, 7131-7135
Ru-MoS_2/CC	1.0 M KOH	41	-	114	*Appl. Catal. B-Environ.* **2019**, 249, 91
Ru@NG-750	1.0 M KOH	40	-	35.9	*ACS Catal.* **2019**, 9, 9897-9904
Ni_5P_4-Ru/CC	1.0 M KOH	54	-	52	*Adv. Mater.* **2020**, 32, 1906972
Ru@SC-CDs	1.0 M KOH	29	-	57	*Nano Energy* **2019**, 65, 104023

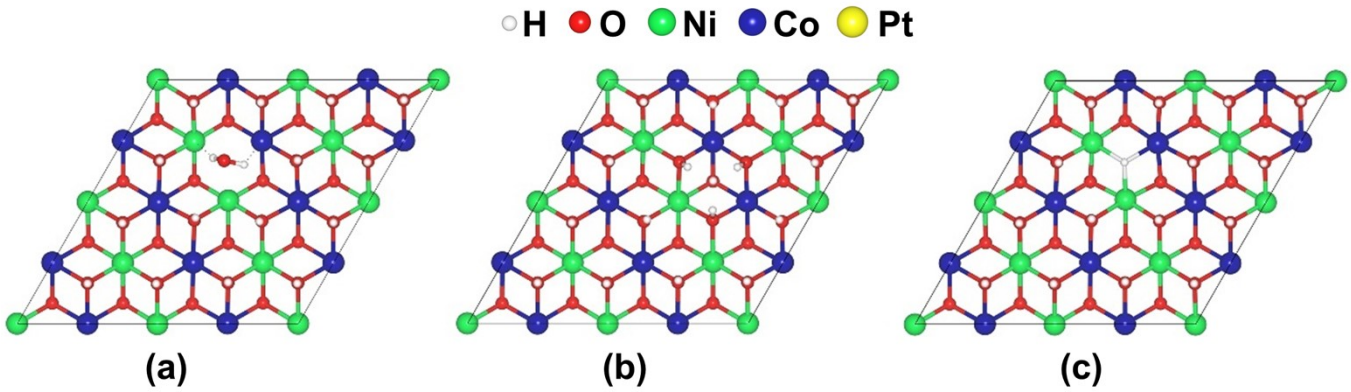

Fig. S17 Atomic structures of intermediates: (a) *H_2O, (b) *OH + *H, and (c) *H, adsorbed on (Ni,Co)$(OH)_2$. The red, green, blue, grey, yellow, and white balls are for O, Co, Ni, Pt, and H atoms, respectively.

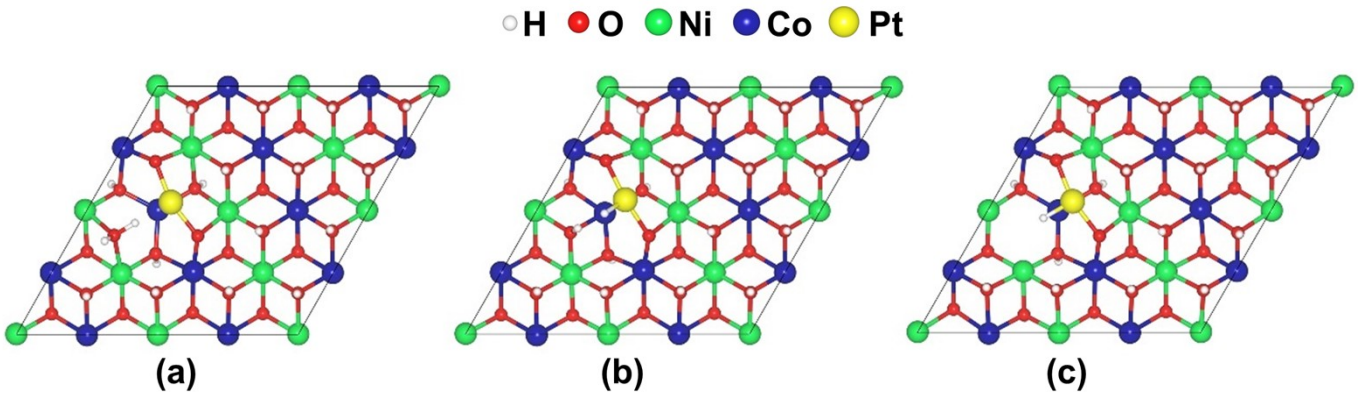

Fig. S18 Atomic structures of intermediates: (a) *H_2O, (b) *OH + *H, and (c) *H, adsorbed on Pt_1/(Ni,Co)$(OH)_2$. The red, green, blue, grey, yellow, and white balls are for O, Co, Ni, Pt, and H atoms, respectively.

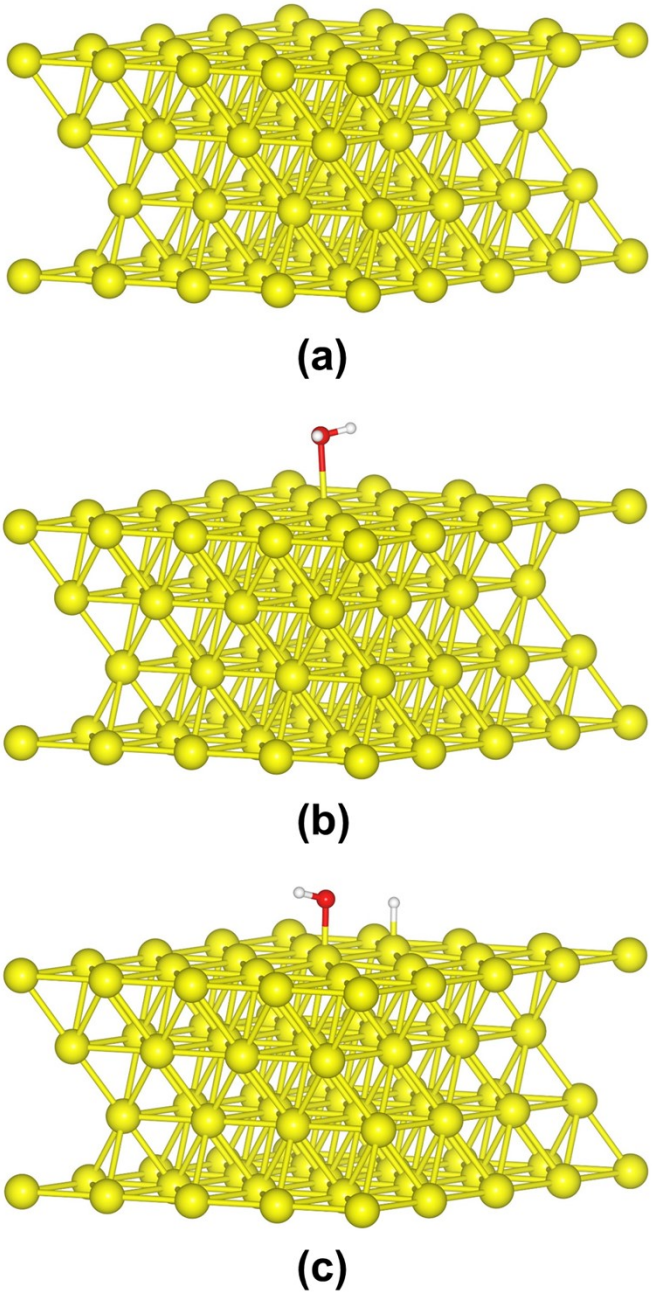

Fig. S19 Atomic structures of intermediates: (a) *H_2O, (b) *OH + *H and (c) *H, on commercial Pt(111). The yellow and white balls are for Pt, and H atoms, respectively.

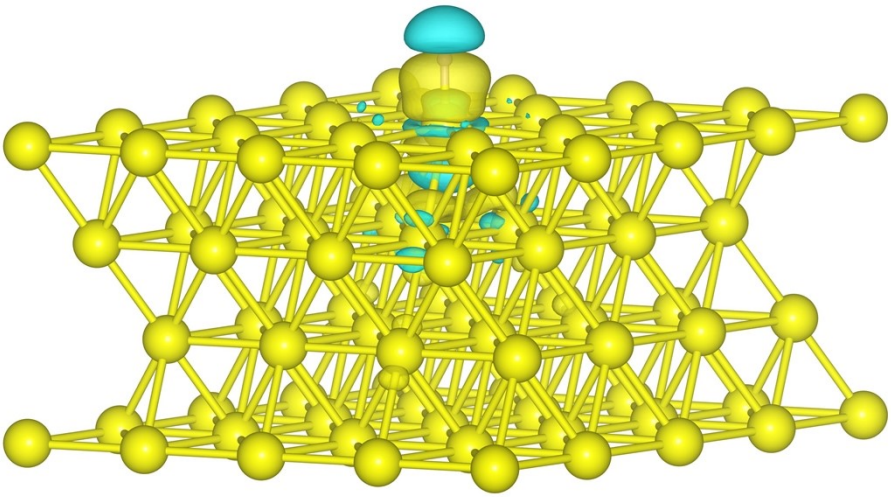

Fig. S20 Charge density difference for the adsorption of one H on Pt(111). Electrons accumulate between Pt and H and deplete on these two atoms which indicate that there is a covalent bond between them. The yellow and white balls are for Pt, and H atoms, respectively. The charge depletion and accumulation were depicted by blue and yellow isosurfaces, respectively.

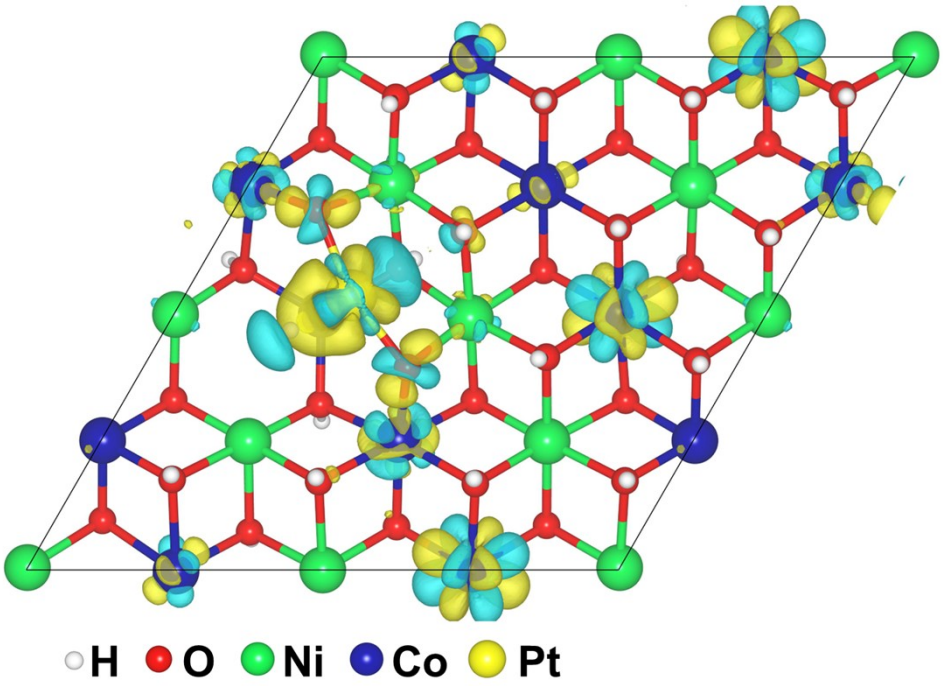

Fig. S21 Charge density difference for the adsorption of one H on Pt_1/(Ni,Co)$(OH)_2$. Electrons accumulate (yellow) between Pt and H and deplete (blue) on the other two metallic atoms, indicating a covalent bond between them. The charge depletion and accumulation were depicted by blue and yellow isosurfaces, respectively.

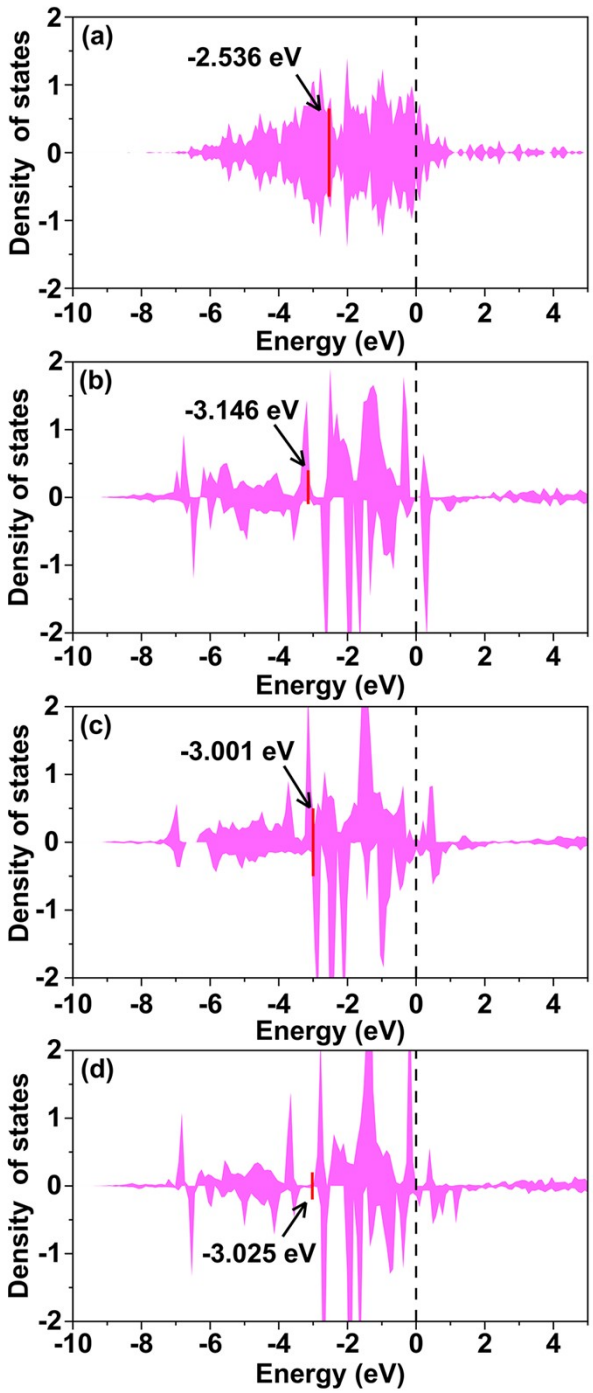

Fig. S22 Density of states for 3*d* states of Pt atoms in (a) Pt(111), (b)$Pt_1/Ni(OH)_2$ (c) $Pt_1/Co(OH)_2$ and (d) $Pt_1/(Co,Ni)(OH)_2$. The energy levels of the *d*-band center of each Pt atom are highlighted by a red line.

References

[1] P. Hohenberg, *et al. Phys. Rev.*, 1964, **136**, 864-871.

[2] G. Kresse, *et al. Phys. Rev. B*, 1996 **54**, 11169-11186.

[3] G. Kresse, *et al. Comp. Mater. Sci.*, 1996, **6**, 15-50.

[4] G. Kresse, *et al. Phys. Rev. B*, 1994, **49**, 14251-14269.

[5] P. E. Blöchl, *Phys. Rev. B,* 1994, **50**, 17953-17979.

[6] J. P. Perdew, *et al. Phys. Rev. Lett.*, 1996, **77**, 3865-3868.

[7] Z. M. Ao, *et al. J. Phys. Chem. C,* 2010, **114**, 14503-14509

[8] A. A. Peterson, *Energy Environ. Sci.*, 2010, **3**, 1311-1315.

[9] H. J. Monkhorst *et al. Phys. Rev. B*, 1976, **13**, 5188-5192.

[10] J. K. Nørskov, *et al. J. Phys. Chem. B.*, 2004, **108**, 17886-17892.

[11] G. L. Chai, *et al. J. Am. Chem. Soc.*, 2014, **136**, 13629-13640.

[12] G. L. Chai, *et al. Energy Environ. Sci.*, 2017, **10**, 1186-1195.

[13] G. L. Chai, *et al. Chem. Sci.*, 2016, **7**, 1268-1275.

[14] L. Su, *et al. Adv. Funct. Mater.,* 2021, **31**, 2104343.

[15] D. Kunwar, *et al. ACS Catal.,* 2019, **9**, 3978-3990.

[16] R. Zhang, *et al*. *Adv. Mater.,* 2016, **29**, 1605502.

[17] K. L. Zhou, *et al. Nat. Commun.,* 2021, **12**, 3783.

[18] X. D. Wang, *et al*. *Energy Environ. Sci.,* 2016, **9**, 1468.

[19] Y. T. Luo, *et al. ACS Nano,* 2018, **12**, 4565-4573.

[20] S. Fang, *et al. Nat. Commun.,* 2020, **11**, 1029.

[21] J. Dai, *et al. Nat. Commun.,* 2020, **11**, 5657.

[22] C. Zhang, *et al. ACS Catal.,* 2018, **8**, 8077-8083.

[23] K. Xu, *et al. ACS Energy Lett.,* 2018, **3**, 2750-2756.

[24] Z. Li, *et al. Adv. Mater.,* 2020, **32**, 7.

[25] D. Baek, *et al. Adv. Funct. Mater.,* 2019, **29**, 8.

[26] C. Hu, *et al. Adv. Sci.,* 2020, **8**, 2001881.

[27] L. Yu, *et al. Nano Energy*, 2018, **53**, 492-500.

[28] D. Zhao, *et al. Angew. Chem. Int. Edit.* 2020, **59**, 8982-8990.

[29] Z. J. Chen, *et al. ACS Catal.,* 2018, **8**, 8866-8872.

[30] N. Yao, *et al. Adv. Energy Mater.,* 2019, **9**, 8.

[31] Q. Shao, *et al. ACS Nano*, 2018, **12**, 11625-11631.

[32] P. Xiong, *et al. Nano Lett.,* 2019, **19**, 4518-4526.

[33] D. F. Cao, *et al. ACS Nano,* 2019, **13**, 11733-11740.

[34] J. Yin, *et al. Angew. Chem. Int. Edit.,* 2019, **58**, 18676-18682.

[35] S. Liu, *et al. Adv. Mater.,* 2020, **32**, 2006034.

[36] Z. J. Zhu, *et al. Adv. Mater.,* 2018, **30**, 7.

[37] M. Zhou, *et al*. *ACS Nano,* 2018, **12**, 4148-4155.